THE ASTROPHYSICAL JOURNAL, 301:708–726, 1986 February 15

MULTIFREQUENCY OBSERVATIONS OF THE SUPERLUMINAL QUASAR 3C 345[1]

JOEL N. BREGMAN,[2] A. E. GLASSGOLD, AND P. J. HUGGINS
New York University

G. NEUGEBAUER,[3] B. T. SOIFER, K. MATTHEWS, AND J. ELIAS
Palomar Observatory, California Institute of Technology

J. WEBB, J. T. POLLOCK,[4] A. J. PICA, R. J. LEACOCK, AND A. G. SMITH
Rosemary Hill Observatory, University of Florida

H. D. ALLER, M. F. ALLER, AND P. E. HODGE
University of Michigan Radio Astronomy Observatory

W. A. DENT, T. J. BALONEK,[5] AND R. E. BARVAINIS
University of Massachusetts

T. P. L. ROELLIG
NASA Ames Research Center

W. Z. WIŚNIEWSKI, G. H. RIEKE, AND M. J. LEBOFSKY
Steward Observatory, University of Arizona

B. J. WILLS AND D. WILLS
University of Texas

W. H.-M. KU
Columbia Astrophysics Laboratory, Columbia University

JESSE D. BREGMAN, F. C. WITTEBORN, AND D. F. LESTER[6]
NASA Ames Research Center

C. D. IMPEY
California Institute of Technology

AND

J. A. HACKWELL
University of Wyoming

Received 1985 April 1; accepted 1985 August 20

ABSTRACT

We have investigated the continuum properties of the superluminal quasar 3C 345 with monitoring studies at radio, optical, infrared, and X-ray frequencies as well as with simultaneous multifrequency spectra extending from the radio through the X-ray bands. Variability occurs more rapidly and with greater amplitude toward shorter wavelengths in the infrared-optical region (0.4–100 μm). Radio outbursts, which appear to follow infrared-optical outbursts by about a year, occur first at the highest frequencies, as expected from optical depth effects, although the peak flux is often reached at several frequencies at once. The beginning of outbursts as defined by millimeter measurements corresponds to the appearance of the three known "superluminal" components. An increase in the X-ray flux during 1979–1980 corresponds to increased radio flux, while the infrared flux changes in the opposite sense.

The multifrequency spectra show that the nearly flat radio continuum steepens at 10^{11}–10^{12} Hz and has a power-law slope of -0.91 ± 0.04 from 350 to 20 μm that steepens to -1.40 ± 0.02 at 20 μm–1200 Å. A "blue bump" is detected at rest wavelengths 4000–1500 Å. The X-ray emission has a flatter slope (-0.7) than the infrared-ultraviolet continuum and lies above an extrapolation of that continuum to X-ray energies. This supports the finding from variability that the X-ray emission is not simply connected to the optical emission. Although the shape of the infrared-ultraviolet continuum is generally preserved during flux variations, slope variations occur and are most common in the ultraviolet region. Most of the total power (3×10^{47} ergs s^{-1}) emerges in the submillimeter-optical region but about one-sixth of the power is emitted at X-ray and radio

[1] In view of the large number of collaborators that are required for multifrequency programs, we list the authors by research groups, but emphasize that each group has made important contributions to the data and analysis of this study.

[2] Work also carried out at the National Radio Astronomy Observatory, which is operated by Associated Universities, Inc., under contract with the National Science Foundation.

[3] Also with the *Infrared Astronomical Satellite* team.

[4] Work also carried out at Appalachian State University.

[5] Work also carried out at Williams College.

[6] Also at the University of Texas.

frequencies. The synchrotron self-Compton model indicates that the plasma responsible for emission near 100 GHz is Doppler boosted ($\delta \approx 3$) has a radius of 0.3 pc, with $B \approx 2$ G and $n_e \approx 10$ cm^{-3}. The energy densities in photons and magnetic fields are comparable and greater than in particles; particle reacceleration is likely.

The emission-line ratios, covering factor, and Lyα equivalent width in 3C 345 are the same as in ordinary quasars. From this result and observations of ordinary quasars, we argue that the ionizing continuum is unbeamed in 3C 345. One model consistent with available data is where the plasma emitting the ionizing radiation is accelerated to relativistic velocities as it moves outward, giving rise to emission at longer wavelengths, and eventually separating from the core as a superluminal component.

Subject headings: infrared: sources — quasars — radiation mechanisms — radio sources: variable — X-rays: sources

I. INTRODUCTION

Understanding the continuum emission in active quasars and BL Lacertae objects requires a detailed study of their fluxes from the radio through the X-ray region. Because these sources are variable, it is necessary to obtain observations across this broad frequency range on time scales shorter than the variability time, and thereby obtain sumultaneous, multifrequency spectra. We have used such observations to determine the connection between the various spectral regions and to estimate the conditions in the emitting plasma in the BL Lacertae object 0735+178 (Bregman *et al.* 1984), the flaring, violently variable quasar 1156+295 (Glassgold *et al.* 1983; Wills *et al.* 1983), the X-ray bright BL Lacertae object I Zw 187 (Bregman *et al.* 1982), and the red quasar 1413+135 (Bregman *et al.* 1981). In this most comprehensive effort to date, these techniques are applied to the violently variable quasar 3C 345, which is distinguished from the sources previously studied by its strong emission lines and the superluminal motion of its milliarcsecond radio components.

The radio source 3C 345 (1641+399), one of the first quasars discovered ($Z = 0.595$; Burbidge 1965), possesses all the properties of the high polarization sources (which include BL Lacertae objects): rapid optical variability, radio variability, large and rapidly variable optical polarization, a steep optical spectrum, and a flat radio spectrum. Perhaps more than any other source, there has been an intense effort to study its radio properties on both small and large scales. The arcsecond-scale structures that dominate the flux at frequencies below 100 MHz are still visible at 5 GHz, although faintly. From a VLA study performed at 1.5 and 5 GHz, Perley, Fomalont, and Johnson (1982) discovered a diffuse halo with a scale of about 15″, and symmetric emission lobes that extend to 2.″8 (14 kpc for $H_0 = 75$ km s^{-1} Mpc^{-1} and $q_0 = \frac{1}{2}$; these cosmological parameters are used throughout). The dominant milliarcsecond radio components are a compact core and a jet, which are most easily distinguished at 2.3, 5.0, 10.7, and 22 GHz (Bååth *et al.* 1981; Cohen *et al.* 1981; Schraml *et al.* 1981; Spencer *et al.* 1981; Readhead *et al.* 1983; Cohen *et al.* 1983*b*; Unwin *et al.* 1983; Cohen *et al.* 1983*a*; Biretta *et al.* 1983; Moore, Readhead, and Bååth 1983). These authors find a "jet" of four distinct components that extends westward from an intense core. Three of these components exhibit superluminal behavior with apparent velocities of 4–11*c*, depending upon the component and epoch. These observations may be interpreted as radiating plasma moving along a curved trajectory that is nearly along our line of sight (with a viewing angle of 2°–3° and a Lorentz factor of about 8; Moore, Readhead, and Bååth 1983). Unlike the jet components, which have flux distributions that peak near or below 1 GHz, the core component has a rising spectrum that probably peaks near 10 GHz (Unwin *et al.* 1983). These suggest that the core is composed of several components that become dominant at higher frequency and give rise to the flat radio spectrum that extends into the millimeter region.

An approach based on multifrequency spectra and long-term monitoring complements the VLBI studies. It allows us to determine whether evidence exists for relativistic motion in wavebands other than the radio, to calculate the physical conditions in the various emitting regions, and to ascertain the connection between the emission in the X-ray, infrared-ultraviolet, and radio regions. The comprehensive monitoring data presented here include optical, infrared, and radio measurements for a period of 20 yr, far-infrared fluxes obtained with the *Infrared Astronomical Satellite* (*IRAS*), and X-ray fluxes taken with the *Einstein Observatory* (§ II). The second aspect of this work is the presentation and discussion of four simultaneous multifrequency spectra. These spectra, which extend from radio to ultraviolet frequencies are analyzed to determine spectral shapes, total power, the connection between the spectral regions, and the details of spectral variation during outbursts (§ III). Simple theoretical considerations are applied to these data to estimate conditions in the emitting region (§ V). The ultraviolet and optical emission lines are compared to those of normal quasars and found to be an important discrimination for the issue of relativistic beaming (§ IV). A discussion of the results completes this report (§ VI).

II. FLUX DENSITY VARIATIONS

Extensive radio, infrared, and optical monitoring of 3C 345 has been conducted during the past 20 yr, *IRAS* observations were obtained in 1983, and X-ray measurements were taken during 1979–1980. These measurements are presented and analyzed here to search for connections between the data sets as well as with VLBI activity.

a) The Radio Region

Observations at 4.8, 8.0, and 14.5 GHz were carried out at the University of Michigan Radio Observatory (Aller and collaborators; Figs. 1*b*, 2) and at 15.5 and 89.6 GHz at Haystack, NRAO, and FCRAO (Dent and collaborators; Figs. 1*a*, *c*). Variations that occur at one of the observed frequencies are usually seen in an adjacent frequency but with some differences: outbursts usually begin later at lower frequencies and sometimes have smaller amplitudes.

The best studied and most dramatic period of activity began in 1978 after 3C 345 reached its lowest flux levels in a decade. The outburst appeared first at 89.6 GHz and progressively later at lower frequencies (Figs. 1*c*, 2); the largest amplitude variation occurred at 15 GHz. The detailed 15 GHz data reveal a series of overlapping outbursts or of variable prolonged particle injection during this active period. At 8.0 GHz, these individual events begin to blend together because of opacity effects,

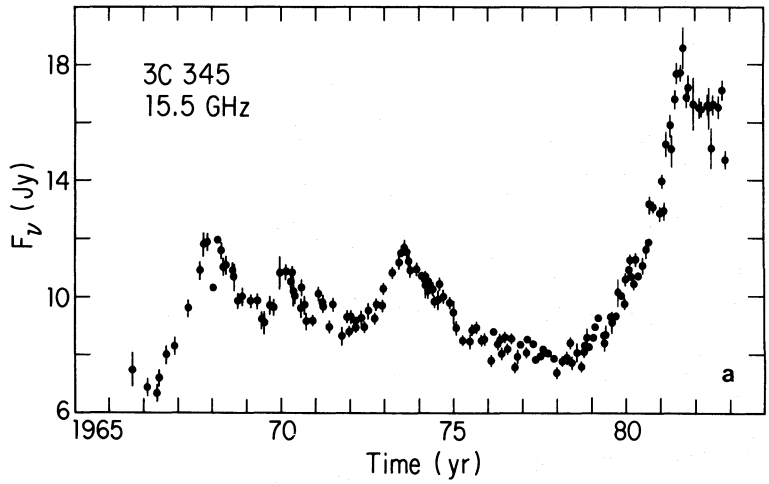

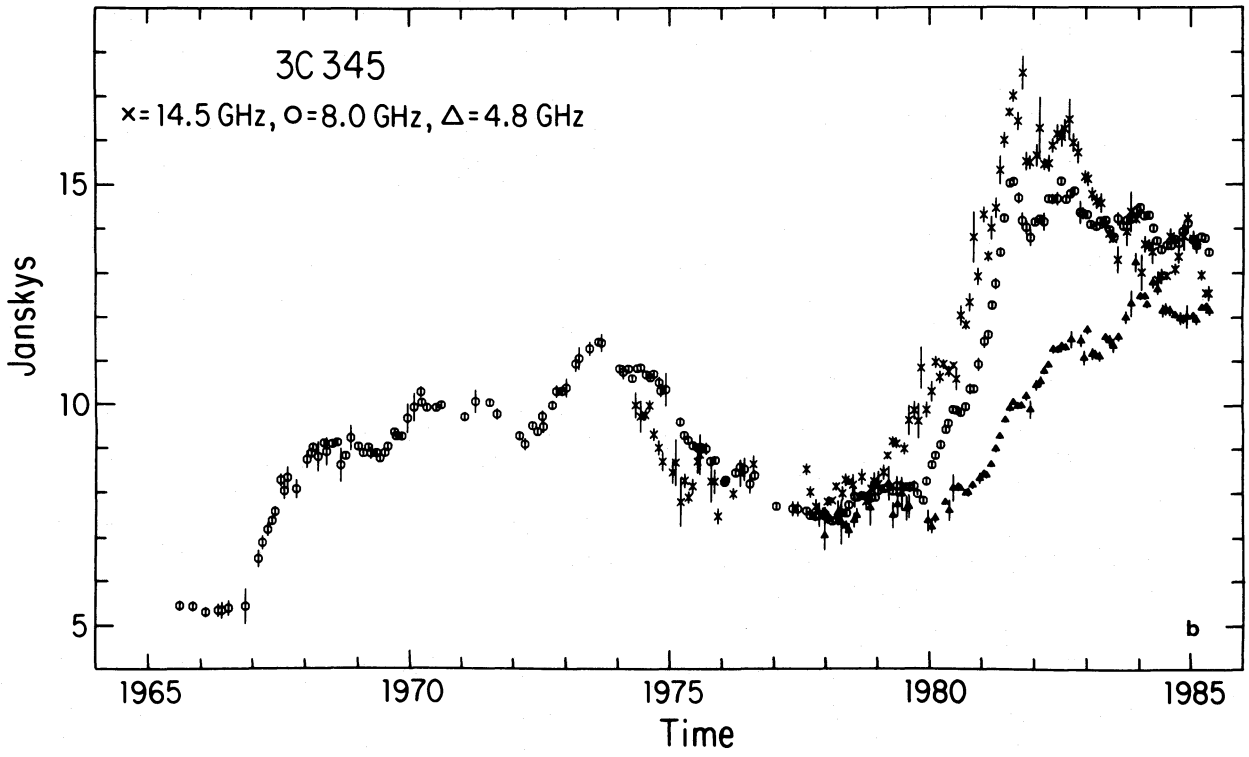

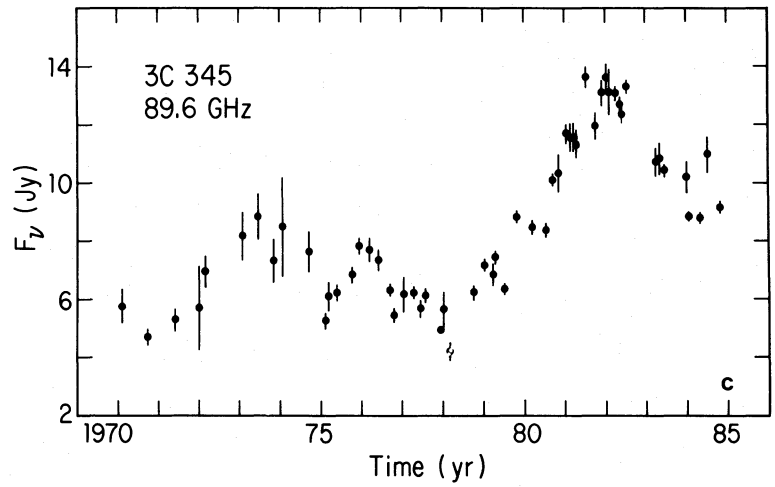

FIG.1.—(*a*) Long-term monitoring of 3C 345 at 15.5 GHz was obtained at Haystack Observatory. (*b*) Plotted on the same horizontal scale as Fig. 1*a* are the monitoring results at 4.8, 8.0, and 14.5 GHz obtained at UMRAO. (*c*) Flux monitoring at 89.6 GHz obtained at FCRAO and NRAO.

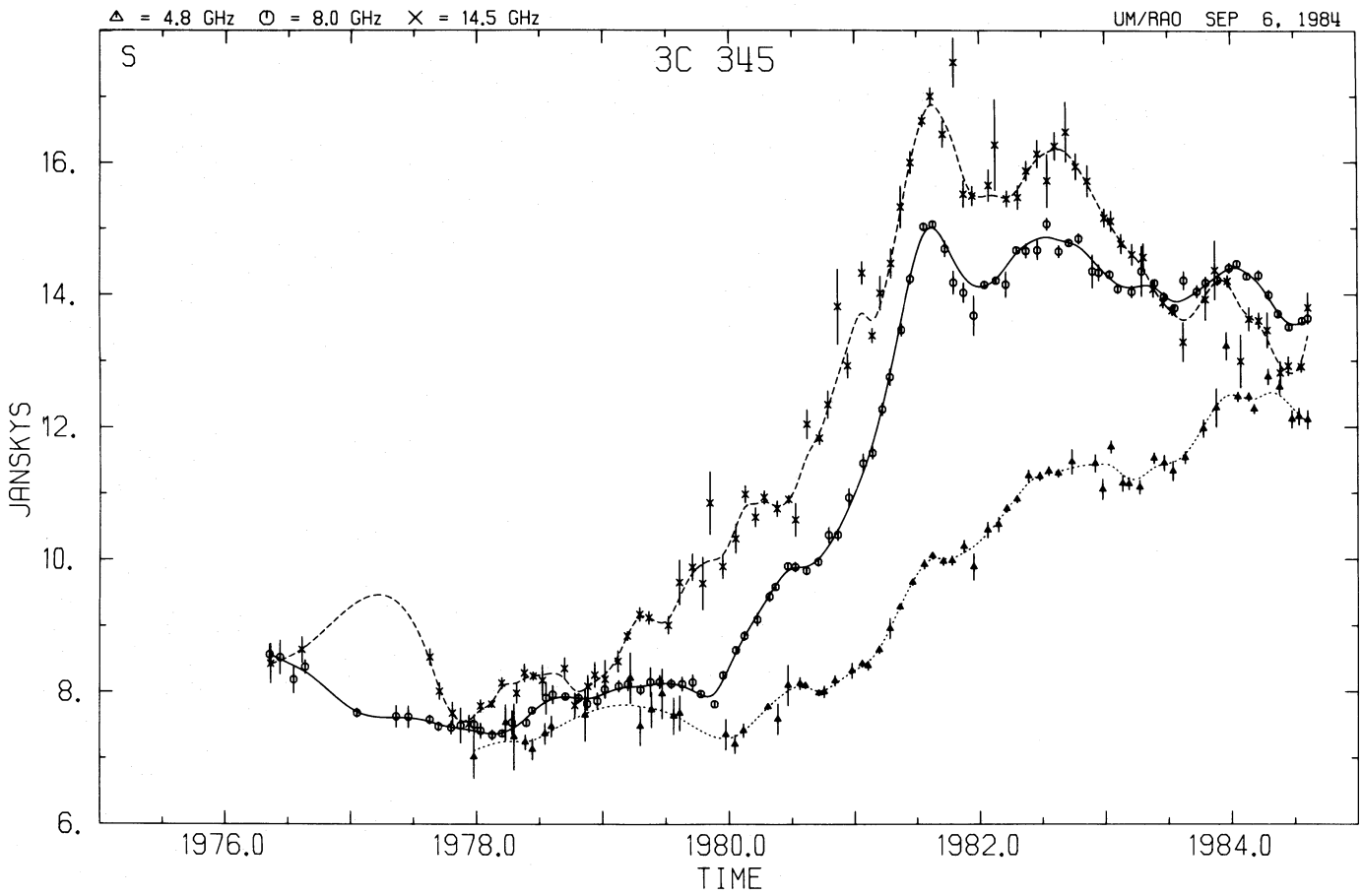

FIG. 2.—This enlargement of the period of recent activity in Fig. 1*b* has been fitted with spline functions

while at 4.8 GHz, opacity effects almost completely mask the existence of many individual events (e.g., the events that peaked in 1981 and 1982 at 14.5 GHz). During 1984 and early 1985 the effects of opacity cause the 4.8 GHz activity to appear totally uncorrelated with the 8.0 and 14.5 GHz variability.

The general picture that arises from the variability data is that the source undergoes repeated outbursts, sometimes with extended periods of particle injection/acceleration, which appear to overlap at the lower frequencies because of opacity effects. The nearly comparable amplitudes and time scales of the variations between 15 and 90 GHz (a six-to-one frequency range) are inconsistent with the simple expanding source model (van der Laan 1966). Models in which the magnetic field and density decrease less rapidly in time than in the expanding source model are more successful at reproducing the observations (e.g., jet models). The frequency dependent delay in the appearance of an outburst is probably determined by the time required for newly injected particles to reach the location where the absorption depth is approximately unity. The very rapid events served at optical frequencies probably emanate from a smaller core region that is opaque at radio frequencies.

The outburst that began in 1978 corresponds to the appearance of a new milliarcsecond-scale superluminal source component. Based upon the positions and proper motion at 10.7 GHz (Biretta *et al.* 1983) and 22 GHz (Moore, Readhead, and Bååth 1983), the time of zero separation for the new component (C4) occurred during 1978–1979, which corresponds to the time at which the dramatic outburst began. The VLBI data show that the most variable component during this period was either the core region (before C4 became distinct; Unwin *et al.* 1983) or C4, the new compact source (Biretta *et al.* 1983).

The times of zero separation for the other superluminal components may also correspond to the onset of radio flux outbursts as defined by the 89.6 GHz data. The time of zero separation of component C2 is estimated to be 1970.4 ± 1.1 (Unwin *et al.* 1983), which is within 1 σ of the onset of the outburst that peaked in 1973.5. Similarly, the time of zero separation of component C3 (1974.9 ± 0.8; Unwin *et al.* 1983) occurs within 1 σ of the beginning of the outburst that peaked at 1976.0. Except for the difference in power, these outbursts are similar to that associated with the appearance of C4. We believe that the near coincidence of three superluminal components with three millimeter-wave outbursts indicates that there is a physical connection between the two phenomena.

b) Optical Monitoring

The quasar 3C 345 is one of the primary targets of an optical monitoring program that was begun nearly 15 yrs ago at the Rosemary Hill Observatory (University of Florida; A. G. Smith and collaborators). The magnitudes are most frequently obtained at 0.44 μm (*B*), but complementary *U* and *V* data were often obtained; the uncertainty in measurements made with the photographic plate technique is 0.05–0.2 mag.

Like many other variable sources, two types of behavior are evident in the optical variability of 3C 345: short-term flickering of up to a magnitude that occurs on a time scale of a few

weeks, and slow secular changes, such as the well-defined rise of about 1 mag in the mean flux level between 1972 and 1982 (Fig. 3). Determining the occurrence and properties of outbursts depends partly upon fortuitous observational opportunities. For example, the outburst in 1982 October was observed closer to its infrared peak than its optical peak (below), whereas the reverse is true for the 1971 October outburst. Between 1971 and 1984, the brightness range at *B* is about 2 mag, which is similar to the range in *U* (Pollock *et al.* 1979) but is about half a magnitude less than the variation in *V* (Fig. 3). This difference may be attributed to the presence of the 3000 Å bump in the *U* and *B* bands and the strong Mg II λ2798 line in the *B* band. If neither of these features vary (Netzer *et al.* 1979), then the nonthermal continuum variability is diluted and measurements at *V* may serve as a more accurate estimate of the changes in the nonthermal source.

Pollock (1982) collected all published optional measurements, and converted them to *B* magnitudes if necessary. His

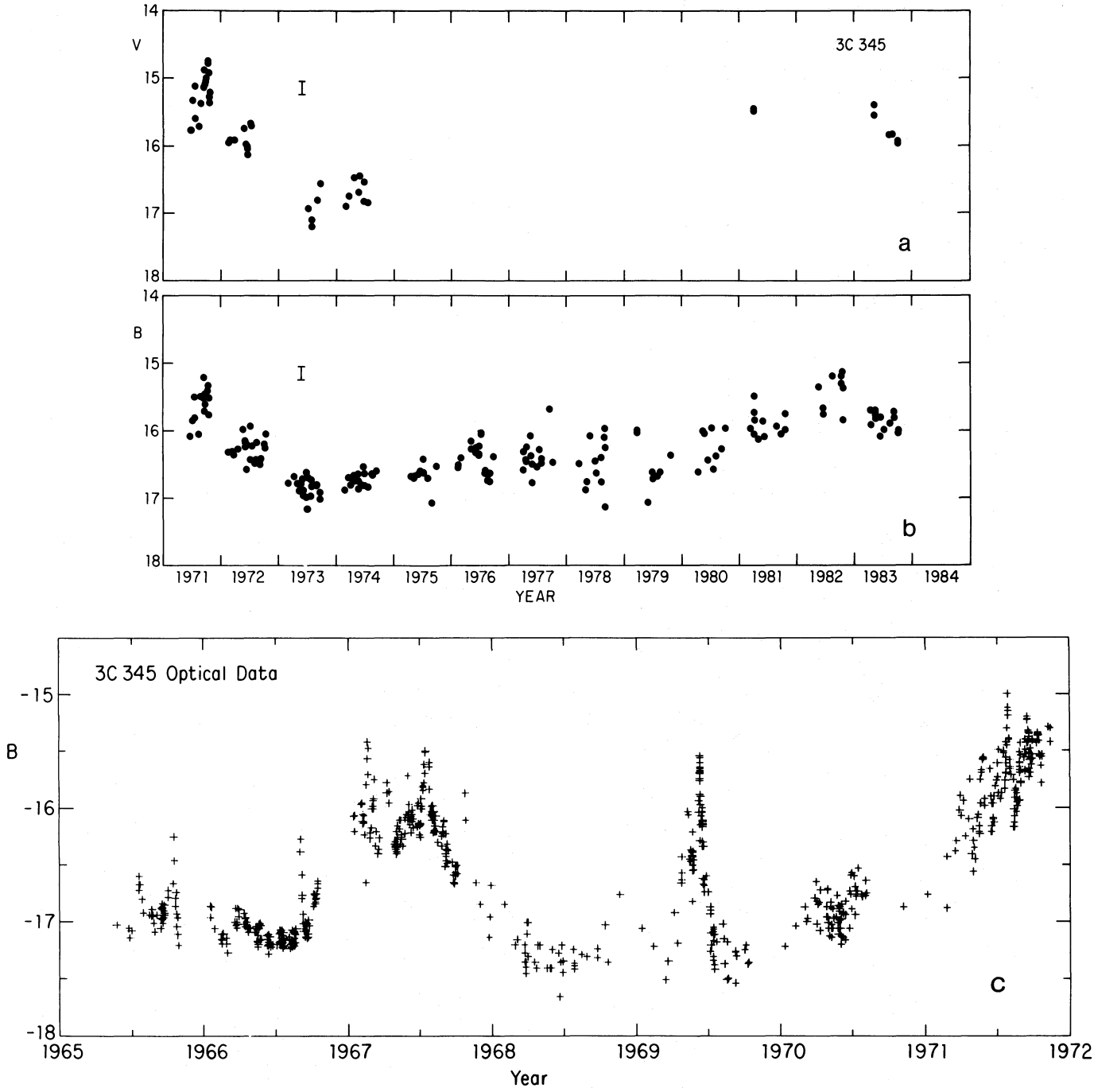

FIG. 3.—(*a*) and (*b*) Optical monitoring from Rosemary Hill Observatory was obtained with the same instrument at both *V* and *B*; typical 1 σ error bars are given toward the left of the diagram. (*c*) All available optical data obtained by several different observers were converted to *B* magnitude. Although some of the data have an error less than 0.05 mag, uncertainties in the color correction may introduce errors as large as 0.3.

data (Fig. 3*c*) show pronounced outbursts in 1967 and 1969 prior to the beginning of the University of Florida monitoring program.

In determining the shortest variability time scale, we consider a flux change to be real only if it is seen in more than one color, or in more than one measurement on a single night or successive nights in a single band; this removes problems associated with occasional plate defects. The half dozen shortest variability events since 1970 have time scales (defined as $dt/d \ln F$) of 3–5 weeks (Fig. 3, Pollock *et al.* 1979; J. R. Webb, private communication). Prior to 1970, variability on similar time scales and possibly as short as 2 weeks have been reported (Lu 1972).

The optical polarization of 3C 345 was large (5%–35%) and variable during 1983.2–1984.5 (Smith *et al.* 1984). They found that the degree of polarization decreases steadily between the *I* and *U* bands; this may be due to the increasing presence of the "blue bump" at shorter wavelength (§ III). The polarization was also proportional to the source brightness during this period, with both decreasing from 1983.2 to 1983.5. A rapid increase in the polarization angle from 15°–30° to 70°–90° occurred at the end of this dimming period (1983.5).

c) Infrared Studies

Monitoring by Neugebauer and collaborators at Palomar Observatory began in 1967 at 1.6 and 2.2 μm, while observations at 1.2, 3.5, and 10.1 μm were obtained regularly after 1975 (Fig. 4). Flickering, secular trends, and outbursts are found in the infrared data that generally correspond to similar optical events. The large infrared outbursts of late 1971 and 1972 October correspond to optical outbursts, although of different amplitude; this may occur because the data sets do not cover the same dates. The range of the 1.2–2.2 μm spectral fluxes is a factor of 15 since 1967, which is slightly greater than that in the *V* band. This difference may occur because the maximum of the infrared range was determined by the 1982 October outburst, and infrared observations were obtained closer to the peak of the outburst than were optical observations.

The most rapid flux variation leads to a variability time scale of about 40 days, but the best defined variability time scale is 56 ± 5 days for the decay following the 1982 October flare. These time scales are longer than those determined from the optical observations. While this difference is probably real, it must be accepted with caution because of less frequent sampling at infrared wavelengths.

Although there is generally good correspondence between the brightness changes in all five infrared bands, the 1982 October outburst was more pronounced at shorter wavelengths (Fig. 5). A quantitative measure of the hardening of the spectrum during the outburst is provided by the spectral slope (Fig. 5), which has a value of -1.25 ± 0.01 during October 1–9, compared to an average value of -1.41 ± 0.02 prior to and following the outburst. If we model the outburst as the addition of a new component to the existing continuum, then the

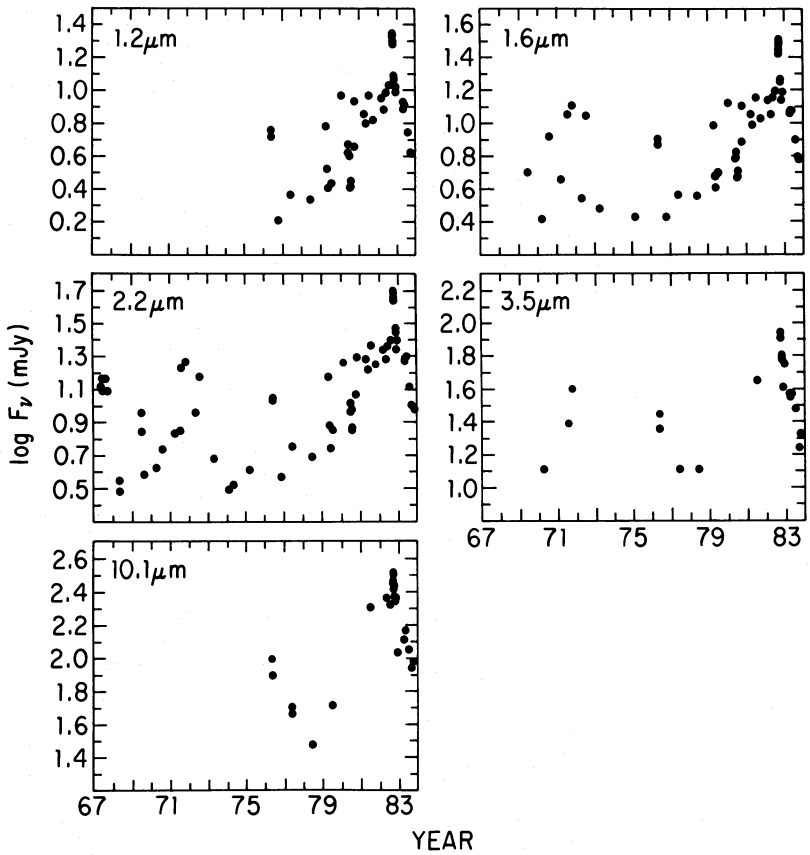

FIG. 4.—Infrared monitoring obtained at Palomar observatory show the same outbursts as at optical wavelengths, although the definition of an outburst often depends upon the time and sampling frequency, which are different for the two data sets. Uncertainties in the measurements are approximately 5%, but are sometimes larger at low flux levels.

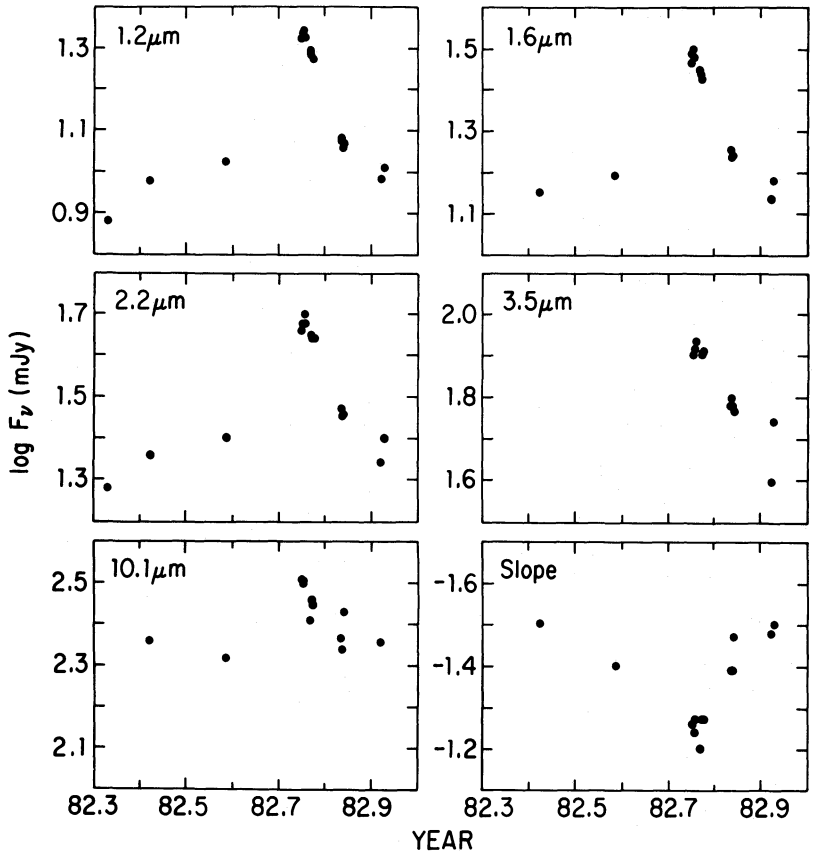

FIG. 5.—An outburst well defined by infrared data shows greater amplitude at short than at long wavelengths

new component has a spectral index of -0.98 ± 0.04. The spectral index of this new component is greater than that of the original spectrum by nearly 0.5, which is the expected difference between a plasma that has suffered synchrotron losses and one that has not. Because the flux decay in the week following the peak is not wavelength dependent, synchrotron losses were not important during this time. Flux variations during the next 2 months are consistent with the simple model where the new component gradually disappears.

A correlation between changes in the hardness and intensity of the spectrum was also observed at longer infrared wavelengths. The *Infrared Astronomical Satellite* (*IRAS*) obtained 43 measurements of 3C 345 in the 12–100 μm region during 1983 (Fig. 6). Between 1983 February–March and 1983 July–September, the flux density decreased and the spectrum became softer (Table 1; Fig. 6). The spectrum between 100 μm and 0.55 μm is curved, steepening at shorter wavelengths so that α (100–25 μm) = -0.68 (February–March), -0.97 (July–September), and α (25–0.55 μm) = -1.31 (February–March), -1.43 (July–September; several optical fluxes were communicated to us in advance of publication by P. S. Smith, R. Landau, and M. Sitko). The spectrum formed from the difference in the flux densities between February–March and July–September has a slope of -1.15 ± 0.04 at 0.55–25 μm but turns over at 60–100 μm. Thus the change in the spectrum can be intrepreted as the dimming of a power-law component that becomes opaque at 60–100 μm. In order for this component to become opaque at these frequencies, it must be smaller and have a larger magnetic field than the remaining component.

d) Connection between Radio, Optical, and Infrared Variation

Several lines of argument suggest that a connection should exist between the activity at radio and infrared-optical wavelengths. The two regions are smoothly connected in the multifrequency spectra (§ III), and theoretical arguments suggest that the plasma radiating at optical wavelengths will eventually diffuse or flow outward to larger scales and radiate in the radio waveband. The unresolved VLBI radio core is smaller than 5 lt-yr in diameter (Spencer *et al.* 1981), and since the plasma moves toward the observer at nearly the speed of light in this region (superluminal motion), the time delay between outburst in optical and radio wavebands should be less than 5

TABLE 1

FLUX DENSITY VARIATION IN 1983

Wavelength	F_ν (Feb–Mar)/F_ν (Jul–Sep)	σ
6 cm	0.97	0.01
4 cm	1.01	0.01
2 cm	1.08	0.01
3.3 mm	1.11[a]	0.03
100 μm	1.08	0.03
60 μm	1.32	0.02
25 μm	1.61	0.03
12 μm	1.72	0.03
2.2 μm	1.9	0.2
0.55 μm	2.6	0.1

[a] Interpolated values used.

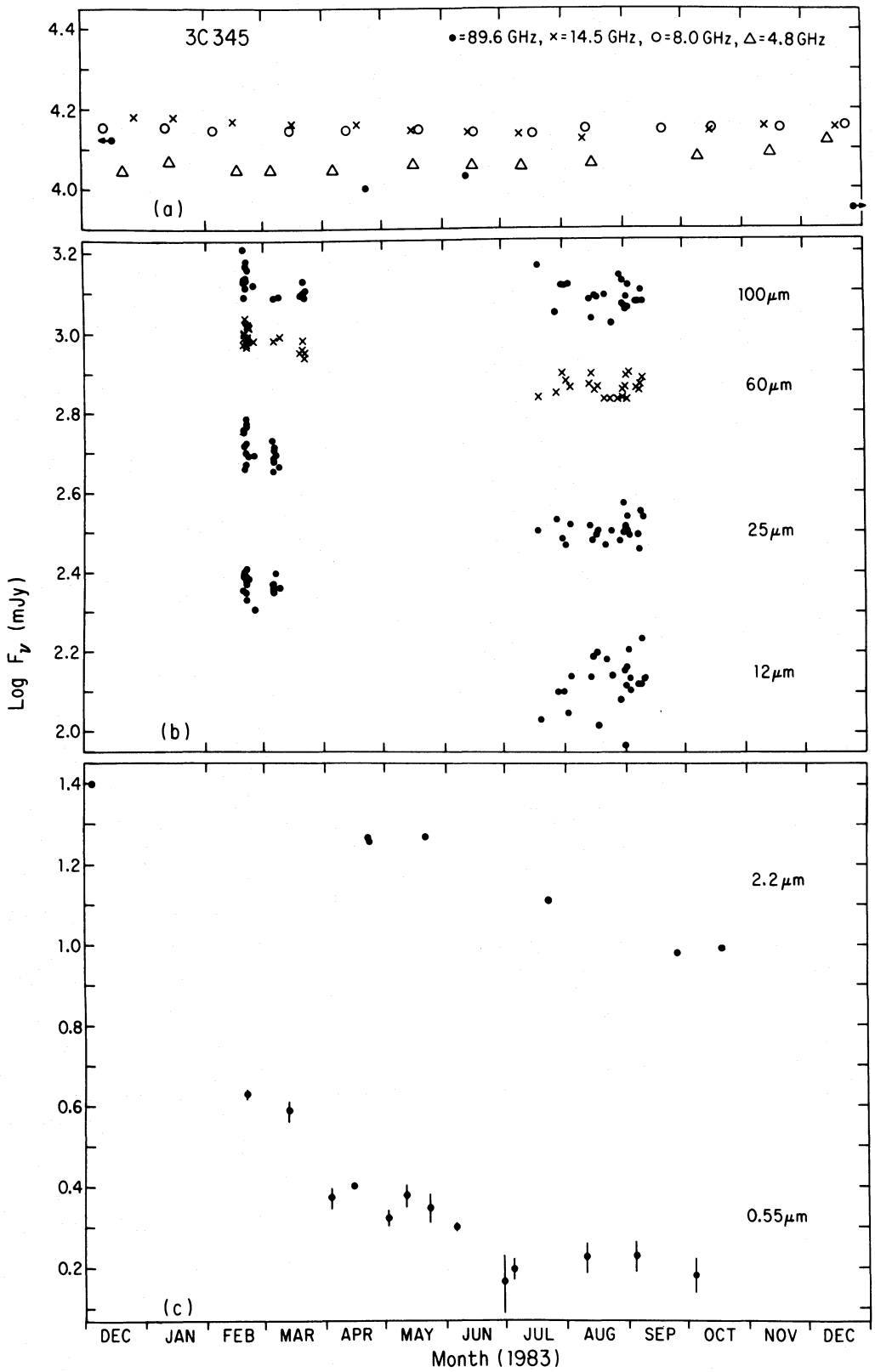

FIG. 6.—Except for the optical data set, measurements at each wavelength were made with a single instrument on the same telescope. Measurement errors less than the 5% are not shown. Uncertainties in the 12–100 μm measurements may be estimated from the scatter of the points during a period of a week.

yr. Although there is not a one-to-one correspondence between radio and infrared-optical variation (with some constant time delay), the three largest infrared-optical outbursts do precede the three largest radio outbursts by roughly 1–2 yr. This result supports the expectation that plasma responsible for infrared-optical emission eventually emerges as radio-emitting plasma.

The relationship between the polarized flux of these two spectral regions is less clear, possibly due to the limited optical and infrared polarization data. The position angle of the optical and infrared data is neither the same as nor 90° different than the radio polarization vector (it is usually in between).

e) X-Ray Studies

As part of a larger program carried out by the Columbia Astrophysics Lab, 3C 345 was observed with the *Einstein Observatory* once during 1979 and on three additional occasions during 1980. The first three images were taken with the Imaging Proportional Counter (IPC), a sensitive instrument that offers spatial resolution of a few arc minutes and some spectral information. The final observation was taken with the High Resolution Imager (HRI), which offers spatial resolution of few arc seconds but provides no spectral information and is less sensitive than the IPC. The data are summarized in Table 2 (the hardness ratio is the number of counts in the 0.8–3.5 keV band minus that in the 0.2–0.8 keV band, all divided by the total number of counts). A spectral slope and a column density of absorbing gas in the Galaxy are fitted to the data. The column density thus calculated is what one would expect based upon H I surveys of the sky; the mean slope is -0.7.

The HRI observations show that the X-ray emission from 3C 345 is pointlike (1″ resolution) and, to within an uncertainty of 1″, coincident with the optical and radio nuclear positions. Short-term variability (100–1000 s) during individual exposures was searched for but not found. However, there is evidence for a general increase in the X-ray emission from 3C 345 during 1980. The third measurement is 31% brighter (3.2 σ) and the last measurement is 50% brighter (3.7 σ) than the first two measurements. No spectral variation was observed.

A comparison may be made between X-ray, optical, infrared, and radio variability. The beginning of the radio outburst coincides with the X-ray brightening and, to within the uncertainty of the X-ray measurements, the increase in the X-ray flux is about the same as the increase in the 15 GHz radio flux. There is also an increase during this period of the optical and infrared fluxes when averaged over 3 month intervals. However, there is no apparent correlation between the X-ray and optical-infrared fluxes when closely spaced observations are compared (in one case, infrared fluxes changed in the opposite sense from the X-ray measurements). Unless variations occur much more rapidly at X-ray than at optical and infrared frequencies, the X-ray emission is probably associated with the radio emitting region rather than with the infrared or optical region.

III. MULTIFREQUENCY SPECTRA

Four multifrequency energy distributions were obtained centered in 1981 April, 1982 October, 1983 May, and 1983 October. Such spectra represent the combined efforts of a large number of observers on different telescopes; the observers, dates of observations, spectral regions, and flux levels are given in Table 3. The data reduction procedures and descriptions of the instruments used can be found in other articles by each of the observers. No correction is made for galactic reddening, which is expected to be insignificant according to Burstein and Heiles [1982; $E(B-V) = 0.00$]. Because the spectrum with the most extensive wavelength coverage was taken in 1983 May, it will be discussed first, and the other multifrequency spectra will be compared to it.

a) The Multifrequency Spectrum of 1983 May

The data for this spectrum were obtained when the infrared and optical flux was decreasing (Fig. 6) and 2 yr after the peak of the radio outburst. As seen in Table 3, the ultraviolet and optical data were taken within a day of May 12, and the radio data were obtained during May 5–12. We have included ground-based submillimeter data taken in April while near-infrared and satellite infrared measurements (*IRAS*) were interpolated from observing periods before and after May 12.

In the radio region, the spectrum is basically flat, although there are significant undulations about a horizontal line which presumably result from the existence of several optically thick sources in the milliarcsecond core (Fig. 7). The 10^{11}–10^{12} Hz region is one of transition where the slope changes from being flat to having a power-law slope of about -1; the source is probably becoming transparent in this region. In the $10^{11.9}$–$10^{13.2}$ Hz region (20 μm–1 mm), the spectrum has a slope of -0.91 ± 0.04, steepening to a slope of -1.40 ± 0.02 in the $10^{13.2}$–$10^{15.4}$ Hz range (1200 Å–20 μm; the "blue bump" has been avoided in calculating this value—see below).

In addition to a nonthermal power-law continuum, most quasars have a "blue bump" in the 1000–4000 Å region (rest frame). Balmer continuum reemission and a forest of Fe II lines probably accounts for most of the flux in the 2000–4000 Å region (Wills, Netzer, and Wills 1985), whereas thermal emission, possibly from an accretion disk, may explain to the flux in this feature at shorter wavelengths (most of the power in the

TABLE 2

X-RAY OBSERVATIONS OF THE 3C 345 FIELD

PARAMETER	DATE			
	1979.02	1980.07	1980.15	1980.64
Instrument	IPC	IPC	IPC	HRI
Sequence number	2060	2061	5694	9261
Observation length (s)	2029	2114	3514	2205
Flux (0.2–3.5 keV) (10^{-12} ergs cm^{-2} s^{-1})	4.4 ± 0.4	4.3 ± 0.4	5.7 ± 0.3[a]	6.5 ± 0.5
Hardness ratio	0.17 ± 0.06	0.11 ± 0.05	0.14 ± 0.04	...
Spectral index	−0.6 ± 0.4	−0.7 ± 0.4	−0.8 ± 0.3	...
Log N_H	20.2 ± 0.4	20.0 ± 0.4	19.8 ± 0.3	...

[a] MPC flux in 2–10 keV band was 9.4×10^{-12} ergs cm^{-2} s^{-1}.

TABLE 3

MULTIFREQUENCY OBSERVATIONS OF 3C 345

Observer	Date (year/month/day)	Region	Observing Band	Raw Data	log ν(Hz)	log F_ν (erg cm^{-2} s^{-1} Hz^{-1})
J.N. Bregman, Glassgold, and Huggins	1981 Apr 8.7	UV(IUE)	1225-1335 Å	4.59(-15)[a]	15.370	-26.60 ± 0.04
			1335-1445 Å	3.49(-15)	15.334	-26.65 ± 0.04
			1725-1845 Å	3.46(-15)	15.224	-26.43 ± 0.03
	1981 Apr 4.7	UV(IUE)	1990-2190 Å	4.56(-15)	15.157	-26.19 ± 0.04
			2190-2390 Å	4.26(-15)	15.117	-26.12 ± 0.04
			2650-2750 Å	4.01(-15)	15.046	-26.01 ± 0.03
			2750-2850 Å	3.98(-15)	15.030	-25.98 ± 0.03
			2850-2950 Å	3.44(-15)	15.014	-26.01 ± 0.03
			3100-3200 Å	3.83(-15)	14.979	-25.90 ± 0.04
	1982 Oct 20.1	UV(IUE)	1225-1335 Å	8.28(-15)	15.370	-26.35 ± 0.04
			1335-1445 Å	8.28(-15)	15.334	-26.28 ± 0.05
			1725-1845 Å	7.86(-15)	15.225	-26.08 ± 0.04
	1982 Oct 20.2	UV(IUE)	1990-2190 Å	7.06(-15)	15.157	-25.98 ± 0.04
			2190-2390 Å	6.91(-15)	15.117	-25.91 ± 0.04
			2650-2750 Å	6.43(-15)	15.046	-25.81 ± 0.03
			2750-2850 Å	6.24(-15)	15.030	-25.79 ± 0.03
			2850-2950 Å	5.79(-15)	15.014	-25.77 ± 0.03
			3100-3200 Å	4.50(-15)	14.979	-25.83 ± 0.05
	1983 May 11.4	UV(IUE)	1225-1335 Å	4.22(-15)	15.370	-26.64 ± 0.04
			1335-1445 Å	4.82(-15)	15.334	-26.51 ± 0.04
			1725-1845 Å	4.41(-15)	15.225	-26.33 ± 0.03
	1983 Oct 9.0	UV(IUE)	1225-1335 Å	6.70(-15)	15.370	-26.43 ± 0.03
			1335-1445 Å	5.94(-15)	15.334	-26.42 ± 0.03
			1725-1845 Å	5.82(-15)	15.225	-26.21 ± 0.03
Webb, Pollock, Pica, and Smith	1981 Apr 9.3	Optical	B	15.85 mag	14.83	-25.69 ± 0.08
			V	15.48	14.74	-25.63 ± 0.04
	1982 Oct 20.2	Optical	B	15.42	14.83	-25.51 ± 0.08
	1983 May 11.1	Optical	B	15.79	14.83	-25.66 ± 0.04
	1983 May 12.0	Optical	U	15.26	14.92	-25.87 ± 0.04
			B	15.79	14.83	-25.66 ± 0.04
			V	15.49	14.74	-25.63 ± 0.04
	1983 May 13.1	Optical	B	15.72	14.83	-25.64 ± 0.06
	1983 Oct 6.0	Optical	U	15.52	14.92	-25.97 ± 0.04
			B	15.93	14.83	-25.72 ± 0.06
			V	15.97	14.74	-25.82 ± 0.04
Wisniewski, Rieke, and Lebofsky	1982 Oct 20	Optical	U	14.95	14.92	-25.74 ± 0.04
			B	15.39	14.83	-25.50 ± 0.02
			V	14.93	14.74	-25.41 ± 0.02
			R	14.24	14.63	-25.25 ± 0.02
			I	14.21	14.52	-25.06 ± 0.02
B.J. Wills and D. Wills	1983 May 1-2	Optical	4000 Å	1.48 mJy	14.88	-25.83 ± 0.02
			5000	1.84	14.78	-25.73 ± 0.02
			5500	2.09	14.74	-25.68 ± 0.02
			6000	2.29	14.70	-25.64 ± 0.02
			6500	2.54	14.66	-25.59 ± 0.02
Impey	1981 Apr 8	Infrared	H	12.7 mJy	14.26	-24.90 ± 0.02
	1981 Apr 5-8		K	19.3 mJy	14.13	-24.71 ± 0.02
Hackwell	1982 Oct 19.1	Infrared	J	12.8 mag	14.38	-24.92 ± 0.04
			H	12.1	14.26	-24.85 ± 0.04
			K	11.0	14.13	-24.60 ± 0.04
			L	9.3	13.92	-24.28 ± 0.04
Neugebauer, Soifer, Matthews, and Elias	1981 Apr 12		J	7.18 mJy	14.38	-25.14 ± 0.02
			H	11.2	14.26	-24.95 ± 0.02
			K	19.1	14.13	-24.72 ± 0.02
	1982 Oct 9		J	18.7	14.38	-24.73 ± 0.02
			H	26.8	14.26	-24.57 ± 0.02
			K	43.5	14.13	-24.36 ± 0.02
			L	81.7	13.91	-24.09 ± 0.02
			N	279	13.48	-23.55 ± 0.02
	1982 Oct 31 -Nov 1		J	11.9	14.38	-24.92 ± 0.02
			H	18.0	14.26	-24.74 ± 0.02
			K	29.5	14.13	-24.53 ± 0.02
			L	61.7	13.91	-24.21 ± 0.02
			N	232	13.48	-23.63 ± 0.02
	1983 Apr 22-23		J	7.99	14.38	-25.10 ± 0.02
			H	11.65	14.26	-24.93 ± 0.02
			K	18.8	14.13	-24.73 ± 0.02
			L	35.7	13.91	-24.45 ± 0.02
			N	128	13.48	-23.89 ± 0.02
	1983 May 21		J	8.02	14.38	-25.10 ± 0.02
			H	11.8	14.26	-24.93 ± 0.02
			K	19.5	14.13	-24.71 ± 0.02
			L	36.3	13.91	-24.44 ± 0.02
			N	145	13.48	-23.84 ± 0.02
	1983 Oct 18		J	4.09	14.38	-25.39 ± 0.02
			H	5.92	14.26	-25.23 ± 0.02
			K	9.51	14.13	-25.02 ± 0.02
			L	20.9	13.91	-24.68 ± 0.02
			N	94.2	13.48	-24.03 ± 0.02

TABLE 3—*Continued*

Observer	Date (year/month/day)	Region	Observing Band	Raw Data	log ν(Hz)	log F_ν (erg cm^{-2} s^{-1} Hz^{-1})
J.D. Bregman, Witteborn, and Lester	1982 Oct 22.2	Infrared	8.65 μm	455 mJy	13.541	-26.34[b]
			8.86 μm	165	13.530	-26.79
			9.07 μm	332	13.519	-26.48
			9.29 μm	308	13.509	-26.51
			9.51 μm	196	13.499	-26.71
			9.72 μm	91	13.489	-27.04
			9.94 μm	646	13.480	-26.19
			10.16 μm	196	13.470	-26.71
			10.38 μm	467	13.461	-26.33
			10.59 μm	411	13.452	-26.39
			10.81 μm	584	13.443	-26.23
			11.03 μm	324	13.435	-26.49
			11.24 μm	232	13.426	-26.63
			11.46 μm	499	13.418	-26.30
			11.68 μm	486	13.410	-26.31
			11.89 μm	269	13.402	-26.57
			12.33 μm	329	13.386	-26.48
			12.76 μm	641	13.371	-26.19
			13.20 μm	412	13.357	-26.39
Werner, Roellig, Becklin, and Impey	1983 Apr 3	Infrared	1.25 μm	6.64 mJy	14.38	-25.18 ± 0.02
			1.65 μm	11.0	14.27	-24.96 ± 0.02
			2.2 μm	15.9	14.13	-24.80 ± 0.02
			3.8 μm	33.4	13.90	-24.48 ± 0.02
			10 μm	94.1	13.48	-24.03 ± 0.05
			20 μm	285	13.18	-23.55 ± 0.09
	1983 Apr 1	Submillimeter	350 μm	4.27 Jy	11.93	-22.37 ± 0.08
	1983 Mar 27	Millimeter	1 mm	7.4 Jy	11.48	-22.13 ± 0.11
Neugebauer, Clegg, Harris, Miley, and Rowan-Robinson	1983 Feb 22 -Mar 22	Infrared (IRAS)	12 μm	233 mJy	13.40	-23.63 ± 0.01
			25 μm	511	13.08	-23.29 ± 0.01
			60 μm	963	12.70	-23.02 ± 0.01
			100 μm	1318	12.48	-22.88 ± 0.01
	1983 Jul 19 -Sep 10	Infrared (IRAS)	12 μm	136	13.40	-23.87 ± 0.01
			25 μm	318	13.08	-23.50 ± 0.01
			60 μm	727	12.70	-23.14 ± 0.01
			100 μm	1224	12.48	-22.91 ± 0.01
Dent, Balonek, and O'Dea	1981 Apr 16	Millimeter	89.6 GHz	11.32 Jy	10.95	-21.95 ± 0.02
	1981 Mar 22		89.6 GHz	11.55	10.95	-21.94 ± 0.02
	1981 Apr 14		31.4 GHz	14.74	10.50	-21.832 ± 0.005
	1982 Jul 14		89.6 GHz	13.3	10.95	-21.88 ± 0.01
	1982 Jul 14		31.4 GHz	15.7	10.50	-21.80 ± 0.01
	1982 Oct 23	Radio	15.5 GHz	17.12	10.19	-21.766 ± 0.008
	1982 Oct 17		7.9 GHz	15.53	9.90	-21.809 ± 0.006
	1983 May 5	Millimeter	91.3 GHz	10.83	10.96	-21.97 ± 0.02
	1983 Jun 14		89.6 GHz	10.4	10.95	-21.98 ± 0.01
	1984 Jan 19		89.6 GHz	8.75	10.95	-22.06 ± 0.01
Aller, Aller, and Hodge	1981 Apr 8-27	Radio	14.5 GHz	14.53 Jy	10.16	-21.838 ± 0.074
	1981 Apr 1-30		8.0 GHz	12.92	9.90	-21.889 ± 0.003
	1981 Apr 5-26		4.8 GHz	9.10	9.68	-21.041 ± 0.066
	1982 Oct-Nov		14.5 GHz	16.81	10.16	-21.774 ± 0.004
	1982 Oct 20		8.0 GHz	14.78	9.90	-21.830 ± 0.004
	1982 Sep-Nov		4.8 GHz	11.45	9.68	-21.941 ± 0.004
	1983 May 10		14.5 GHz	14.08	10.16	-21.852 ± 0.005
	1983 May 12		8.0 GHz	14.17	9.90	-21.849 ± 0.003
	1983 May 7		4.8 GHz	11.54	9.68	-21.938 ± 0.004
	1983 Oct 5		14.5 GHz	13.66	10.16	-21.865 ± 0.005
	1983 Oct 9-10		8.0 GHz	14.22	9.90	-21.847 ± 0.003
	1983 Oct 8		4.8 GHz	11.99	9.68	-21.921 ± 0.005

[a] Units: ergs cm^{-2} s^{-1} Å^{-1}.
[b] Errors given in Fig. 9.

bump is from this component; Grandi 1982; Malkan 1983). Emission from a blue bump near 3000 Å was seen in optical spectra of 3C 345 (Oke, Shields, and Korycansky 1984), but it does not vary despite changes in the nonthermal continuum (Netzer *et al.* 1979). Our observations, which include ultraviolet data, permit a study of the blue bump at shorter wavelengths. We find that a bump is apparent near log $\nu = 14.7$–15.3 (1000–4000 Å in the rest frame), which is evident when examining the power per logarithmic frequency interval (the lower curve in Figure 7). Its properties are difficult to measure accurately, but the bump rises approximately 20%–25% above a power law connecting the near-infrared and ultraviolet regions in the 1500–3000 Å region (rest frame). The slope between the near-infrared region and the 1300 Å region (800 Å rest frame) is -1.40 ± 0.03, which is the same as that found from the infrared data alone and supports the idea of an underlying power law upon which the blue bump is seen.

Simultaneous X-ray data are not available for any of the multifrequency spectra, so the average X-ray measurement made with the *Einstein Observatory* has been used in Figure 7.

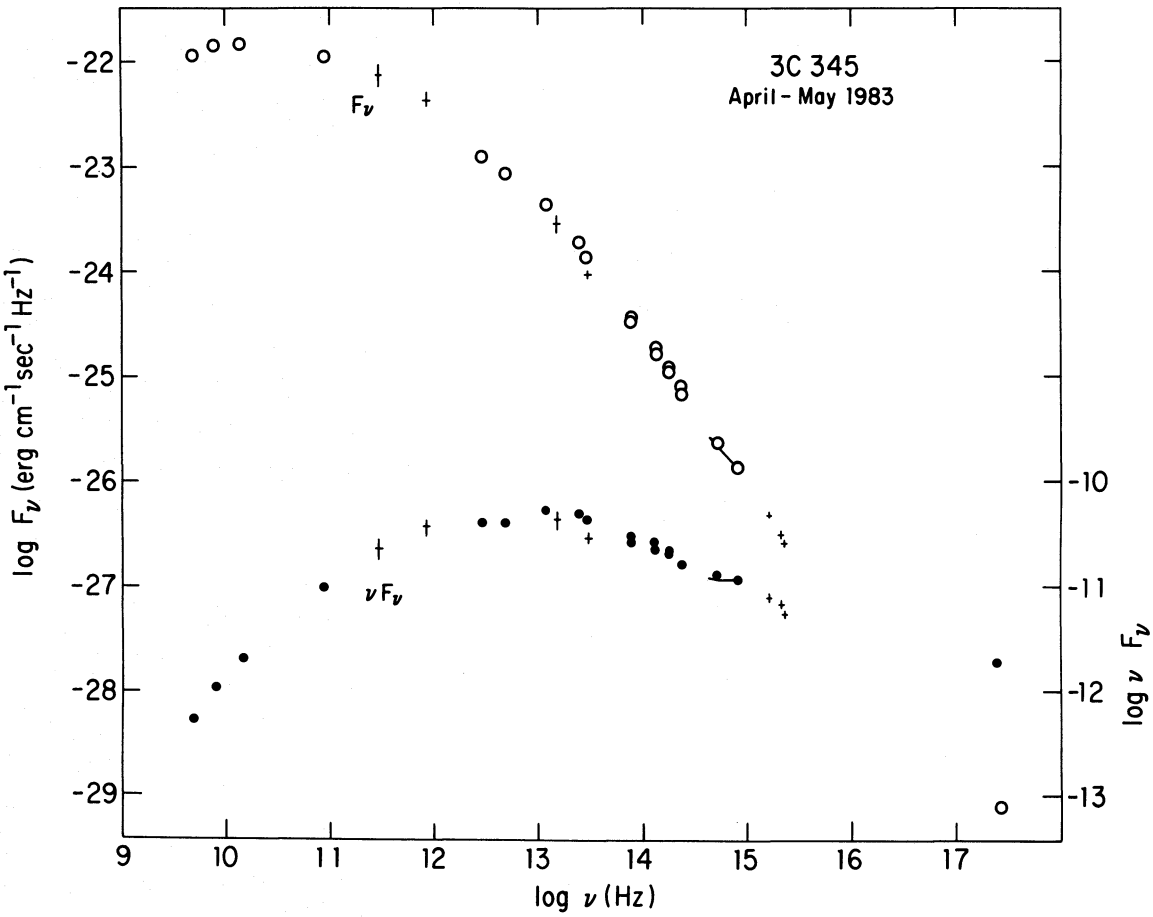

FIG. 7.—The flux density (*top curve, left scale*) and the flux per logarithmic bandwidth (*lower curve*) are shown for the multifrequency spectrum of 3C 345 of 1983 May. All quantities are in the observer's frame. Only the X-ray datum is not simultaneous. One sigma errors greater than 5% are shown.

This is likely to be an underestimate of the true X-ray flux because the source was fainter at optical and radio wavelengths when the X-ray measurements were taken than in 1983 May. A line connecting the ultraviolet (1280 Å) and X-ray (1 keV) data has a slope of -1.23, which is shallower than the infrared-ultraviolet slope (-1.40 ± 0.03), or the ultraviolet slope as determined from more complete *IUE* measurements of 1981 April and 1982 October (-1.95 ± 0.16 and -1.59 ± 0.10, respectively). Because the X-ray data would lie above an extrapolation of the ultraviolet or the infrared-ultraviolet continuum, we conclude that the X-ray emission either comes from a separate region or is created by a different emission process than the infrared-ultraviolet flux. A separate origin for the X-ray flux is further supported by the lack of coordinated variability with infrared emission (§ II*d*) and from the slope of the X-ray data, $\alpha \approx -0.7$, which is different than the slope in the infrared-ultraviolet region.

The power from 3C 345 is broadly distributed through the submillimeter and infrared regions (Fig. 7), with a slow decline in the near-infrared through ultraviolet region. Little power emerges in the radio region, and the power per logarithmic bandwidth in the X-ray region is only 0.04 of the peak value achieved at infrared wavelengths. Even if 3C 345 had the "universal" X-ray spectral slope for active galactic nuclei of -0.62 up to 165 keV (Rothschild *et al.* 1983), it would have a total integrated flux of 4×10^{-11} ergs cm^{-2} s^{-1}. This estimate for the flux is still only one-sixth of the integrated millimeter-ultraviolet flux, 2.6×10^{10} ergs cm^{-2} s^{-1} (1 mm–1200 Å). The flux in the flat radio spectrum, 4×10^{-11} ergs cm^{-2} s^{-1} (4.8–300 GHz), is similar to the estimate for the X-ray flux. The flux in the blue bump is 2.2×10^{-12} ergs cm^{-2} s^{-1}, about 0.65% of the total power emitted in all wavebands. Using the above estimates, the total power (4.8 GHz–165 keV) is 2.9×10^{47} ergs s^{-1}, if emitted isotropically ($H_0 = 75$ km s^{-1} Mpc^{-1} and $q_0 = \frac{1}{2}$).

b) Multifrequency Spectra at Different Epochs

The other multifrequency spectra are analyzed for spectral and flux variation by dividing by the 1983 May spectrum. This procedure is straightforward in the 4.8 GHz to 12 μm range; only a 31.4 GHz point needed to be interpolated in the 1983 May spectrum. For the 12 μm–1200 Å waveband, the spectrum was approximated by the function $F_\nu = 23.9(\nu/10^{14}\ \mathrm{Hz})^{-1.40}$ mJy. The dispersion of a single point about this line is 0.04 in log F_ν.

i) 1981 April Spectrum

Relative to 1983 May, 3C 345 varied by less than a factor of 3 at all frequencies (Fig. 8). During 1981 April, the source was about 20% brighter in the 2.2 μm–2300 Å range with similar spectral slope. A sharp turnover occurs in the ultraviolet waveband, producing a slope (-1.95 ± 0.16) that is steeper than the one characterizing the infrared-optical region. The steepness of the ultraviolet spectrum is caused partly by the presence of the

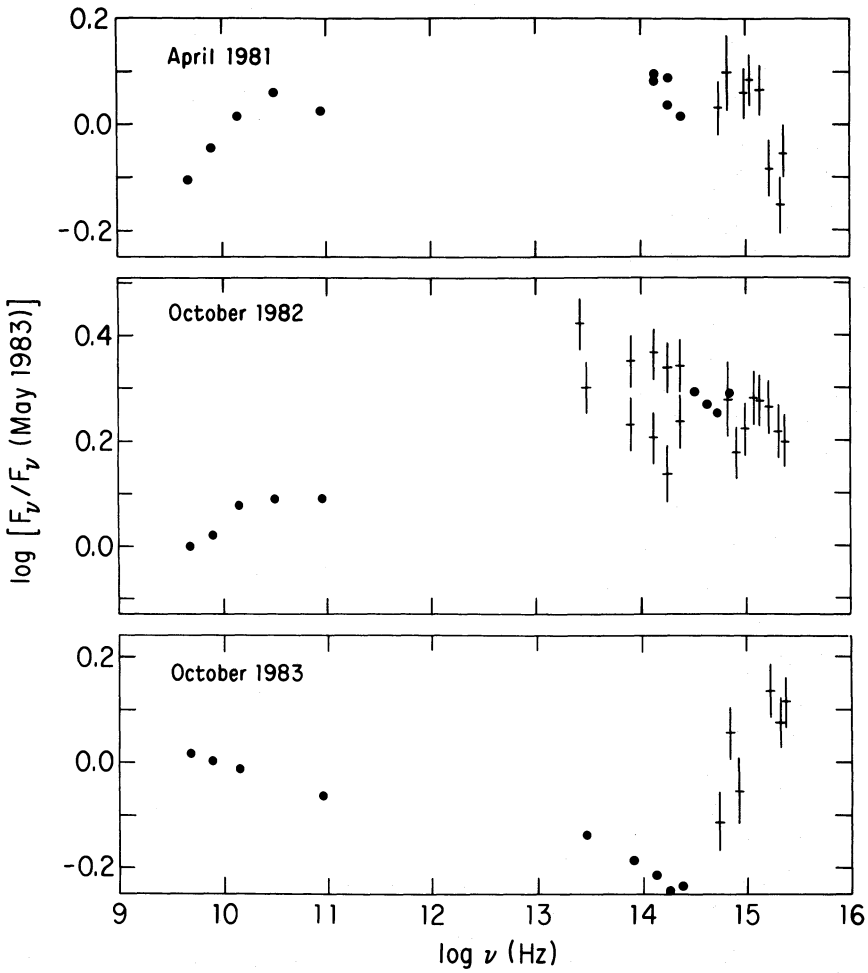

FIG. 8.—Flux densities from the multifrequency spectra of 1981 April, 1982 October, and 1983 October (*top to bottom*) have been divided by the multifrequency spectrum of 1983 May. One sigma errors in excess of 5% are shown.

blue bump in the long wavelength camera of the *IUE*. The radio spectrum was taken just before the outburst peaked at 31.4 GHz and 14.5 GHz, but while it was still rising at lower frequencies; hence, the spectrum is considerably more inverted (positive slope) than in 1983 May.

ii) *1982 October Spectrum*

In 1982 October, shortly after an outburst identified from infrared measurements, 3C 345 was brighter than during any other epoch. Of the two sets of near-infrared flux measurements, the fainter one is probably systematically low due to atmospheric conditions and the calibration chosen; the brighter fluxes are more reliable. The spectral index of the infrared data is the same as in 1983 May but spectral steepening occurs at shorter wavelengths; the slope in the 1200–3100 Å region recorded by the *IUE* is -1.59 ± 0.10. Because the blue does not change brightness with the continuum, its contribution to the flux in the long-wavelength camera of the *IUE* decreases as the source brightness. This is probably why the ultraviolet spectrum is harder in 1982 October than in 1981 April.

An 8.6–13.2 μm spectrum was obtained 2 days after most of the near infrared-ultraviolet data were taken (Fig. 9). At these wavelengths (5–8 μm in the rest frame), dust can give rise to resonant emission excited by ultraviolet photons, and ice mantels on cold dust have absorption features at 6.0 and 6.8

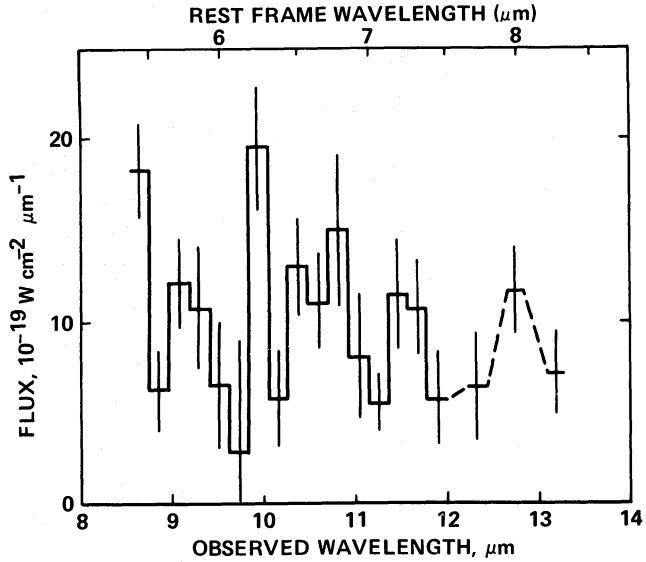

FIG. 9.—The 8.4–13.6 μm spectrum taken during 1982 October along with 1 σ errors is shown in both observed and rest frame wavelengths. No evidence for dust is seen.

μm (Aitken 1980). No such emission features are present in our spectrum. Harvey, Wilking, and Joy (1982) did not find emission from cold dust at long infrared wavelengths, although it might be difficult to detect such a contribution against the bright nonthermal continuum.

A second, broader radio outburst occurred throughout much of 1982, about a year after the initial radio outburst. The radio spectrum of 1982 October was taken shortly after the peak fluxes were reached at 14.5 GHz and 8.0 GHz. The spectrum, which is slightly inverted, is typical of the behavior associated with outbursts (O'Dea, Dent, and Balonek 1985).

iii) *1983 October Spectrum*

The decrease in the infrared and optical fluxes during the first half of 1983 abated by the latter part of the year (Fig. 6). The infrared spectrum is softer and dimmer than in 1983 May, although the spectrum hardens in the ultraviolet region. As the radio flare matured, the fluxes decreased at higher frequencies but increased at lower frequencies, giving rise to a spectrum with negative slope and presumably higher turnover frequency. turnover frequency.

iv) *Summary of the Multiple Epoch Spectra*

Spectral variation is greatest in the ultraviolet region and may be caused by the appearance and disappearance of new components with flatter spectra (which have less effect at longer wavelengths) and by the presence of a nonvariable blue bump. More subtle spectral variation occurs at infrared wavelengths with changes in α generally less than 0.1. There is a general correlation between the highest frequency radio measurements and the infrared measurements, which is consistent with there being a connection between the two spectral regions.

IV. ULTRAVIOLET AND OPTICAL EMISSION LINES

The redshift of 3C 345 (0.595) is such that only one strong line, Mg II λ2798, is easily detected in the optical region. Ultraviolet observations provide a richer bounty: the important emission lines of Lyα, Lyβ + O VI λ1035, C IV λ1549, and C III] λ1909 are accessible with the *IUE*. Figure 10 shows the *IUE* spectrum, with clear detections of Lyα, Lyβ + O VI λ1035, C IV λ1549, and a weak detection of C III λ1909. The very strong Lyα line, at 1940 Å, is near the upper wavelength limit of the short-wavelength camera at 1975 Å. Part of the red wing of Lyα (and N V λ1240) falls beyond the limits of the short-wavelength camera, and the long-wavelength camera is insensitive at these wavelengths. Consequently, the Lyα flux was estimated by doubling the contribution of the blue half of the line, which appears to be symmetric within the central 3600 km s^{-1}; no estimate of the N V λ1240 strength is possible. The uncertainty in the strength of Lyα is 10%–20%, and there is a similar uncertainty for Lyβ + O VI λ1035 and C IV λ1549, which have lower signal-to-noise ratios, but are better placed in the *IUE* spectrum. The largest uncertainty occurs for C III] λ1909, which lies near an insensitive part of the long-wavelength camera. Analyses of two spectra indicates uncertainties as large as 50%. When the problematic C III] λ1909 line is excluded, no line variability is present, despite a factor of 2 variation in the continuum flux.

The important lines of Hβ and Mg II λ2798 were measured in the optical region during 1983 May (Wills and Wills) with uncertainties of 10%–20% (Fig. 11). The measurement of the Hβ flux is the same as that found by Oke, Shields, and Korycansky (1984), but there is a factor of 2 difference in the determination of the Mg II λ2798 flux. Our measurement for Mg II λ2798 is similar to that found by Netzer *et al.* (1979), by Wampler (1967), and by Wills and Wills (unpublished, 1984). Line fluxes are listed in Table 4A.

The optical and ultraviolet line ratios for 3C 345 (Table 4B) are compared with mean values for quasars (col. [3]) and the range of observed values (col. [4]) as determined by Kwan and Krolik (1981; Table 6). The line ratios in 3C 345 are indistinguishable from ordinary quasars.

The fraction of ionizing radiation that should be absorbed to produce the Lyα line (the covering factor) can be calculated provided that the standard models for broad emission-line clouds apply. Model calculations indicate that one ionizing photon produces approximately one Lyα photon and that the broad emission-line clouds lie about a light decade from the central source for 3C 345 (e.g., Kwan and Krolik 1981). During the past 20 yr, the time-averaged flux is 1.3 mJy at 0.44 μm as deduced from Pollock (1982). We assume that the ratio between the optical and the ultraviolet ionizing flux measured in the multifrequency spectra is the same as the time-averaged ratio; the mean ionizing continuum flux is then calculated. Our analysis of the multifrequency spectra indicates that the nonthermal continuum, rather than the "blue bump," is the primary contributor to the ionizing flux; more precise ultraviolet observations could confirm this point. If the clouds see the same radiation as the observer, approximately 10%–30% of the ionizing flux must be absorbed by the broad line gas to produce the observed Lyα. This is similar to the covering factors found by Kinney *et al.* (1985) for a sample of nonvariable intermediate redshift quasars (covering factor of 4%–47% with a mean of 17%). Alternatively, the ratio of the Lyα luminosity to that at 1450 Å (rest frame), which is related to the covering factor, is similar to that for normal quasars of comparable luminosity (Kinney *et al.* 1985).

The finding that the line and continuum properties of 3C 345 resemble normal quasars has important implications for the degree to which the continuum emission can be relativistically boosted and made directional (the combination is referred to

TABLE 4A

EMISSION-LINE FLUXES

Line (1)	Flux (10^{-13} ergs cm^{-2} s^{-1}) (2)
Lyβ + O VI λ1035	1.0 ± 0.2
Lyα	3.4 ± 0.4
C IV λ1549	2.1 ± 0.3
C III λ1909	1.0 ± 0.3
Mg II λ2798	0.92 ± 0.14
Hβ	0.44 ± 0.06

TABLE 4B

EMISSION-LINE RATIOS

Ratio (1)	3C 345 (2)	Quasar Mean[a] (3)	Quasar Range[a] (4)
Lyα/Hβ	7.7 ± 1.5	6.8	2.2 –16.4
(O VI λ1035 + Lyβ)/Lyα	0.29 ± 0.07	0.24	0.10– 0.56
C IV λ1549/Lyα	0.62 ± 0.11	0.36	0.15– 0.64
C III] λ1909/C IV λ1549	0.5 ± 0.2	0.51	0.14– 0.84
Mg II λ2798/Hβ	1.7 ± 0.3	1.60	0.34– 2.4

[a] Compiled by Kwan and Krolik 1981.

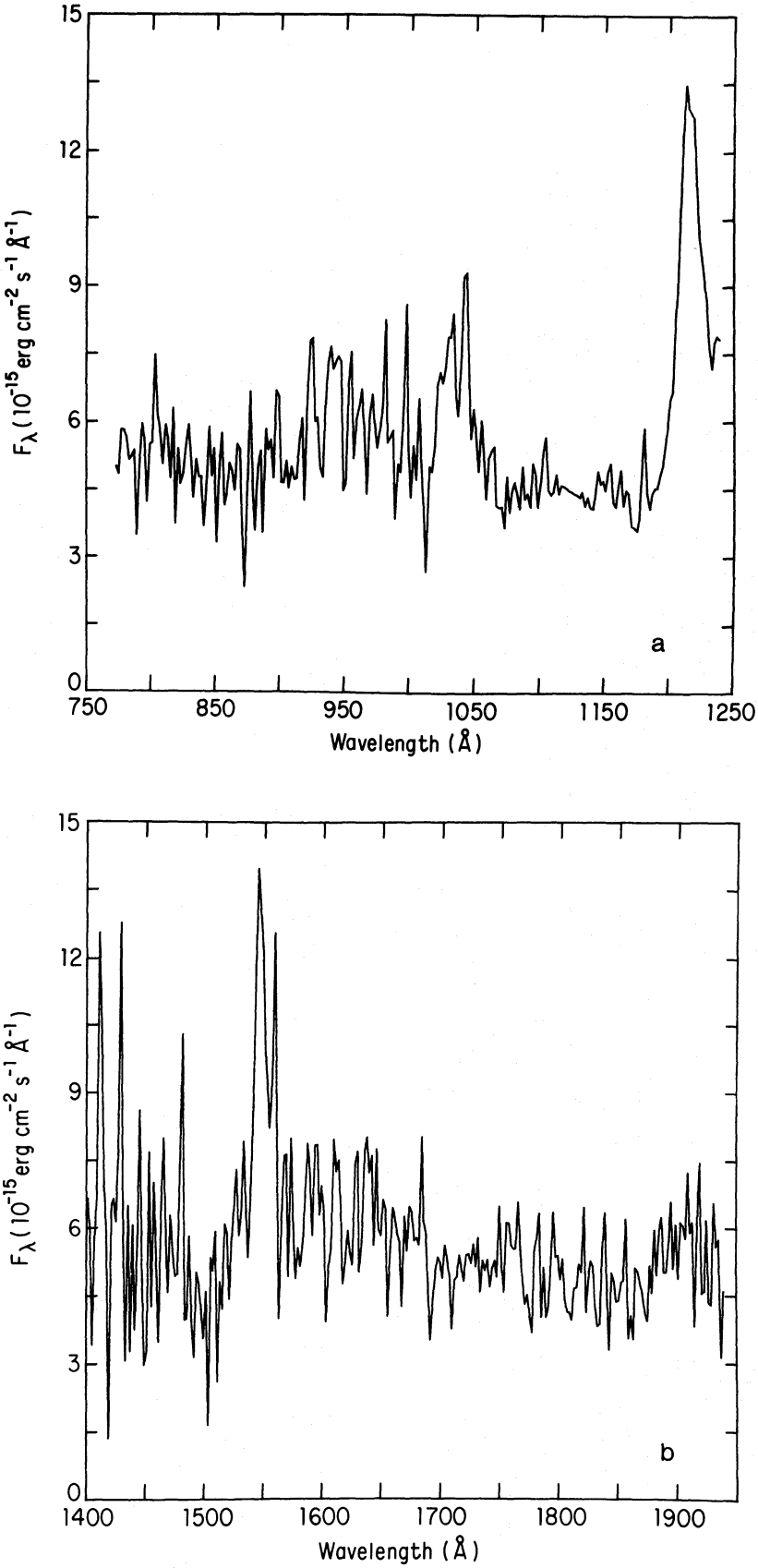

FIG. 10.—(*a*) Two sets of *IUE* spectra have been averaged and shifted to their rest frame wavelengths. The common quasar lines of Lyβ + O VI λ1035, Lyα, C IV λ1550, and C III] λ1909 are present in this spectrum.

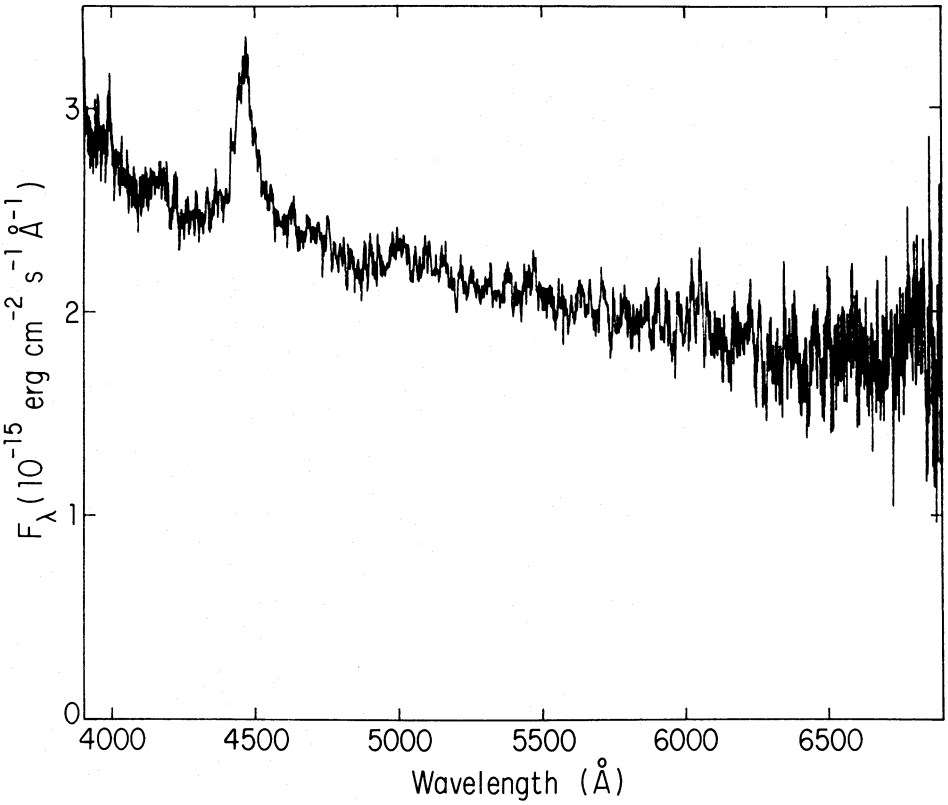

FIG. 11.—Optical spectrophotometry in 1983 May shows the Mg II λ2798 line; the wavelength scale is in the observer's frame

as beaming). For ordinary quasars, Kinney *et al.* (1985) found little dispersion about the relationship between the luminosity at Lyα and at 1450 Å. Because beaming of the continuum would increase the dispersion in such a diagram, they argued that the Lorentz factor associated with relativistic beaming of the ionizing continuum must be small ($\Gamma < 1.15$). Since the line properties of 3C 345 are indistinguishable from normal quasars then, by analogy, the ultraviolet continuum emission in 3C 345 is not substantially beamed. This argument does not rule out emission that is relativistically boosted but isotropic (as from a relativistically expanding shell).

V. THE PHYSICAL CONDITIONS IN THE EMITTING REGION

The conditions within the continuum emitting region (the magnetic field, size density, and bulk motion) can be calculated by applying a model to the data, such as the synchrotron self-Compton model (e.g., Jones, O'Dell, and Stein 1974; Marscher 1983). In doing so, it is necessary to define the structure of the emitting regions of interest.

One interpretation of the data is that the flat radio spectrum arises from a series of partly optically thick regions (suggested by VLBI observations) and that the steepening of the spectrum at frequencies above 100 GHz occurs because the source becomes completely transparent. In addition to knowing the flux density and frequency at which the source is transparent, three additional parameters must be known in order to apply the homogeneous synchrotron self-Compton model: the spectral index in the optically thin region (approximately -1 at 10^{11}–10^{13} Hz), the observed variability time scale (1 yr at 90 GHz), and the inverse Compton flux density (assumed to be the X-ray emission). Model calculation that were made from the 1983 May multifrequency spectrum yield: $r \approx 0.3$ pc, $B \approx 2$ G, $n \approx 10$ cm^{-3} (a minimum electron energy of 15 MeV was assumed), and $\delta \approx 3$, where δ is the Doppler boosting parameter given by

$$\delta = \frac{[1 - \beta^2]^{1/2}}{[1 - \beta \cos \theta]},$$

and θ is the angle to our line of sight ($\theta = 0$ for approaching sources). The estimates for the magnetic field and size are fairly insensitive to uncertainties in the variability time scale, slope of the electron distribution, or the inverse Compton flux; the determination of the density depends sensitively upon several input quantities. The energy density of the photons and the magnetic field are comparable, but the energy density in particles is 10^2–10^3 times lower. The radiative lifetime is less than the light travel time across the source, so local reacceleration may be present.

Other models have been developed that include the effects of changing plasma parameters with distance (Condon and Dressel 1973; Marscher 1977; Blandford and Königl 1979; Marsher 1980; Königl 1981; Reynolds 1982*a*, *b*). At the radius where the source becomes transparent, some of the plasma parameters calculated with these models may differ from the homogeneous model (for example, the magnetic field can be smaller than the value we calculated by an order of magnitude). In practice, these models are more difficult to apply because several new parameters are introduced, some of which strongly influence the results but are not fundamental quantities like the magnetic field (i.e., an inner and outer radius of the volume). However, these models offer a way of under-

standing the spectral shape in the partly optically thick radio region that is not too sensitive to additional parameters. For 3C 345, the nearly flat spectrum implies that $n \approx 2$ and $m \approx 0.8$, where $B = B_0(r/r_0)^{-m}$ and the density parameter $K = K_0(r/r_0)^{-n}$ (Marschen 1977; Königl 1981).

Acceleration of the emitting plasma, which has been considered by some authors (Marscher 1980; Reynolds 1982*a*, *b*), may be an important effect in 3C 345. For the region in which the ionizing continuum originates, the bulk motion must be small (Lorentz factor of motion ≈ 1) in order to be in harmony with the argument based upon emission-line strengths (§ IV). At long wavelengths (and larger length scales), VLBI measurements of the core reveal considerable relativistic motion ($\delta \approx 4$–11) (Unwin *et al.* 1983). Because our data suggest that plasma emitting optical radiation eventually becomes radio-emitting plasma, a consistent picture is one in which the emitting plasma accelerates as it moves outward.

An important observational constraint for theoretical models is the wavelength-dependent variability at 100–0.55 μm (§ II). As mentioned above (§ II), this could arise from a new component with a spectral index flatter by 0.5 than the typical 20 μm–0.12 μm spectrum; this plasma may not have yet been affected by radiative losses. Eventually, radiative losses should occur and the difference in the spectral index of 0.5 between 100–20 μm and 20–0.12 μm is consistent with this expectation. However, improved theoretical models that include realistic flows are badly needed in order to make detailed comparisons with observations.

VI. SUMMARY

The behavior of the continuum emitting region of 3C 345 has been investigated through an analysis of four multifrequency spectra; long-term optical, infrared, and radio monitoring; and X-ray observations.

Optical monitoring shows flickering on a time scale as short as a few weeks (dt/d ln F), superposed upon slower baseline changes that take place over years. The infrared monitoring (1.2–10.2 μm) shows variability generally similar to that in the optical but with some important differences. During an outburst, the amplitude of variation was greater at 1.2–2.2 μm than at 10.2 μm. Also, the variability time scale becomes progressively shorter, going from 10.2 μm to 0.55 μm. The *IRAS* observations indicate that this trend continues at longer wavelengths and that the variation at 100 μm is nearly an order of 0.55 μm. These results suggest at least two emitting regions: one with $\alpha \approx -1.0$, and the other with $\alpha = -1.4$. In addition, synchrotron losses are probably important.

Radio monitoring data lack the short-term variations comparable to optical flickering but reveal outbursts lasting a few years, such as the event that began in 1978–1979. This outburst began at millimeter frequencies, with lower frequencies responding later. However, the peak flux was reached at about the same time at frequencies between 8 GHz and 90 GHz. The appearance of a new superluminal component, C4, is associated with the beginning of the outburst as defined by the millimeter-wave measurements. The additional coincidence between zero separation for the two older superluminal components, C2 and C3, and the beginning of the other two millimeter-wave outbursts in the 1970s, suggests a correspondence between the creation of new components and millimeter outbursts. There is also a correspondence between optical and radio outbursts in which optical outbursts precede the radio events by about a year. This behavior is expected for plasma moving outward and expanding: It appears first at high frequencies where the plasma is transparent (optical region), and later, when it has expanded and the optical depth at low frequencies has decreased, a radio outburst is observed (partly opaque emission). Eventually, this plasma separates from the central region as a superluminal component.

Only four X-ray measurements exist, but they were obtained at the beginning of the recent radio outburst. The X-ray fluxes showed a modest increase that is proportional to the increase at radio wavelengths. In contrast, infrared measurements taken near two of the X-ray observations indicate that these two wavebands are not directly coupled.

On four separate occasions, nearly simultaneous multifrequency observations were obtained that include observations in some or all of the following wave bands: radio, millimeter, submillimeter, far-infrared, near-infrared, optical, and ultraviolet regions. The most complete spectrum of the group, taken in 1983 May, shows a flat radio continuum that steepens at 10^{11}–10^{12} Hz. The spectrum between 350 μm (10^{12} Hz) and 20 μm has a slope of -0.91 ± 0.04, but this steepens to a slope of -1.40 ± 0.02 in the 20 μm–1200 Å range. In addition to the nonthermal power-law spectrum, a "blue bump" is evident in the spectrum at 4000–1500 Å (rest frame). This is probably caused by a combination of Fe II lines, Balmer continuum reemission, and blackbody radiation at 10,000–40,000 K. An extrapolation to higher energies of the nonthermal 12 μm–1200 Å spectrum, or of the spectrum determined from the ultraviolet data alone (which is steeper), would pass well below the X-ray datum, suggesting that the X-rays are not simply an extension of the optical emission (consistent with the variability findings and the flatter X-ray spectrum, $\alpha = -0.7$). When the various multifrequency spectrum are compared, it is found that the radio spectrum exhibits the complex behavior expected from partly optically thick sources undergoing an outburst. Changes in the infrared-optical spectrum are simpler. The spectrum generally retains its shape as the flux level changes, although spectral variation often occurs at ultraviolet wavelengths and less frequently at infrared wavelengths. Some, but not all, of the ultraviolet spectral variability is linked to the presence of the nonvariable "blue bump" at one end of the *IUE* wave band.

The flux from the source is broadly distributed in the submillimeter through optical regions. The X-ray flux, even if it extends out to 165 keV without spectral steepening, is only about one-sixth of that from the submillimeter-optical region. The radio and X-ray fluxes are similar, while the flux in the "blue bump" is $<1\%$ of that in the submillimeter-optical region. The total power in 1983 May was 2.9×10^{47} ergs s^{-1} if the radiation is emitted isotropically.

The emission lines of Lyα, Lyβ + O VI λ1035, C IV λ1549, and C III] λ1909 were identified and measured in the ultraviolet spectra, which extend to 770 Å (rest frame). The broad emission line clouds should cover approximately 20% of the 4π sr surrounding the source in order to absorb enough ionizing radiation to account for the Lyα flux. This value for the covering factor and the measured line ratios are similar to those in ordinary nonvariable quasars. Kinney *et al.* (1985) have argued that the ionizing continuum in nonvariable quasars is not relativistically beamed and, because the line properties of 3C 345 are indistinguishable from ordinary quasars, we suggest that the ionizing continuum in 3C 345 is also not beamed.

Finally, the physical conditions within the emitting regions were calculated using synchrotron self-Compton models. The

break in the radio spectrum near 100 GHz is interpreted as the frequency at which the source becomes completely transparent. We calculate that the plasma responsible for the emission near 100 GHz is characterized by $\delta \approx 3$, $B \approx 2$ G, $r \approx 0.3$ pc, and $n \approx 10$ cm^{-3}. The energy density in the emitting region is dominated by the photons and the magnetic field, with the particle energy density about two orders of magnitude lower. Local particle acceleration is suggested because the synchrotron loss time is shorter than the light crossing time of the emitting region. In comparison, the 5–10 GHz VLBI measurements reveal an unresolved core less than 5 lt-yr in diameter with $B > 1$ G and $\delta \approx 4$–11 (the density is very uncertain; larger resolved components have lower values of B and n). Thus, although the radio size is probably much larger than the region responsible for the infrared emission, the magnetic field is only a slowly decreasing function of size.

Our analysis indicates a fundamental difference between the plasma radiating $\nu < 100$ GHz, where the radiation is beamed, and the ionizing continuum, which was argued is not beamed. Acceleration of the plasma along a jet could explain this, and such models have been suggested by Benford (1978), Marscher (1980), and Reynolds (1982*a*, *b*). An important test of these models is whether they can reproduce the variability observed in the transparent region (>100 GHz). We hope that the observations presented here will encourage investigators to study the signature of flux variability associated with these models.

Special thanks are extended to Mike Werner and Eric Becklin for their role in obtaining the extensive infrared data of 1983 May. These investigators and T. Roelling wish to thank the infrared group at Caltech and Palomar Observatory for their support and assistance in obtaining 1 mm observations. We also wish to thank G. Miley, P. Clegg, M. Rowan-Robinson, and S. Harris for their efforts in establishing and carrying out the active galaxy-pointed observations with *IRAS*. R. Landau, M. Sitko, and P. S. Smith made optical data available to us prior to publication. In addition, many of the optical monitoring observations were obtained by G. H. Folsom, R. L. Hackney, K. R. Hackney, R. L. Scott, P. L. Edwards, B. Q. McGimsey, P. Gombola, and G. L. Fitzgibbons as part of an ongoing program at the University of Florida (supported by the NSF, current grant AST-8400208). H. D. Aller and M. F. Aller would like to thank the NSF for their support of the University of Michigan Radio Observatory (grant AST-8301234). C. D. Impey acknowledges the SERC for observing support and receipt of a SERC/NATO Fellowship. Financial support was provided to W. W. Wiśniewski, G. H. Rieke, and M. J. Lebofsky from the NSF; B. J. Wills and D. Wills from the NSF; J. N. Bregman, A. E. Glassgold, and P. J. Huggins from NASA; J. Hackwell from the NSF; J. D. Bregman, F. C. Witteborn, and D. F. Lester from NASA; T. P. L. Roellig from NASA; G. Neugebauer from NSF; W. A. Dent, T. J. Balonek, and R. E. Barvanis NSF; W. H.-M. Ku from NASA.

REFERENCES

Aitken, D. K. 1980, in *IAU Symposium 96, Infrared Astronomy*, ed. C. G. Wynn-Williams and D. P. Cruikshank (Dordrecht: Reidel), p. 207.
Aller, M. F., and Aller, H. D. 1984, *Bull. AAS*, **16**, 957.
Bååth, L. B., *et al.* 1981, *Ap. J.* (*Letters*), **243**, L123.
Benford, G. 1978, *M.N.R.A.S.*, **183**, 29.
Biretta, J. A., Cohen, M. H., Unwin, S. C., and Pauliny-Toth, I. I. K. 1983, *Nature*, **306**, 42.
Blandford, R. D., and Königl, A. 1979, *Ap. J.*, **232**, 34.
Bregman, J. N., *et al.* 1984, *Ap. J.*, **276**, 454.
Bregman, J. N., *et al.* 1982, *Ap. J.*, **253**, 19.
Bregman, J. N., Lebofsky, M. J., Aller, M. F., Rieke, G. H., Aller, H. D., Hodge, P. E., Glassgold, A. E., and Huggins, P. J. 1981, *Nature*, **293**, 714.
Burbidge, E. M. 1965, *Ap. J.*, **142**, 1674.
Burstein, D., and Heiles, C. 1982, *A.J.*, **87**, 1165.
Chanan, G. A., Margon, B., and Downes, R. A. 1981, *Ap. J.* (*Letters*), **243**, L5.
Cohen, M. H., *et al.* 1983*a*, *Ap. J.*, **272**, 383.
Cohen, M. H., Unwin, S. C., Pearson, T. J., Seielstad, G. A., Simon, R. S., Linfield, R. P., and Walker, R. C. 1983*b*, *Ap. J.* (*Letters*), **269**, L1.
Cohen, M. H., Unwin, S. C., Simon, R. S., Seielstad, G. A., Pearson, T. J., Linfield, R. P., and Walker, R. C. 1981, *Ap. J.*, **247**, 774.
Condon, J. J., and Dressel, L. L. 1973, *Ap. Letters*, **15**, 203.
Glassgold, A. E., *et al.* 1983, *Ap. J.*, **274**, 101.
Grandi, S. A. 1982, *Ap. J.*, **255**, 25.
Harvey, P. M., Wilking, B. A., and Joy, M. 1982, *Ap. J.* (*Letters*), **254**, L29.
Jones, T. W., O'Dell, S. L., and Stern, W. A. 1974, *Ap. J.*, **192**, 261.
Kinney, A. L., Huggins, P. J., Bregman, J. N., and Glassgold, A. E. 1985, *Ap. J.*, **291**, 128.
Königl, A. 1981, *Ap. J.*, **243**, 700.
Kwan, J., and Krolik, J. H. 1981, *Ap. J.*, **250**, 478.
Lu, P. K. 1972, *A.J.*, **77**, 829.
Malkan, M. A. 1983, *Ap. J.*, **268**, 582.
Marscher, A. P. 1977, *Ap. J.*, **216**, 244.
Marscher, A. P. 1980, *Ap. J.*, **235**, 386.
———. 1983, *Ap. J.*, **264**, 296.
Moore, R. L., Readhead, A. C. S., and Bååth, L. 1983, *Nature*, **306**, 44.
Netzer, H., Wills, B. J., Uomoto, A. K., Rybski, P. M., and Tull, R. R. 1979, *Ap. J.* (*Letters*), **232**, L155.
O'Dea, C. P., Dent, W. A., and Balonek, T. J. 1985, in *Active Galactic Nuclei*, ed. J. E. Dyson (Manchester: Manchester University Press), p. 63.
Oke, J. B., Shields, G. A., and Korycansky, D. G. 1984, *Ap. J.*, **277**, 64.
Perley, R. A., Fomalont, E. B., and Johnston, K. J. 1982, *Ap. J.* (*Letters*), **255**, L93.
Pollock, J. T. 1982, Ph.D. thesis, University of Florida.
Pollock, J. T., Pica, A. J., Smith, A. G., Leacock, R. J., Edwards, P. L., and Scott, R. L. 1979, *A.J.*, **84**, 1658.
Readhead, A. C. S., Hough, D. H., Ewing, M. S., Walker, R. C., and Romney, J. D. 1983, *Ap. J.*, **265**, 107.
Reynolds, S. P. 1982*a*, *Ap. J.*, **256**, 13.
———. 1982*b*, *Ap. J.*, **256**, 38.
Rothschild, R. E., Mushotzky, R. F., Baity, W. A., Gruber, D. E., Matteson, J. L., and Peterson, L. E. 1983, *Ap. J.*, **269**, 423.
Schraml, J., Pauliny-Toth, I. I. K., Witzel, A., Kellermann, K. I., Johnston, K. J., and Spencer, J. H. 1981, *Ap. J.* (*Letters*), **251**, L57.
Smith, P. S., Balonek, T. J., Heckert, P. A., and Elston, R. 1984, *Bull. AAS*, **16**, 952.
Spencer, J. H., Johnston, K. J., Pauliny-Toth, I. I. K., and Witzel, A. 1981, *Ap. J.* (*Letters*), **251**, L61.
Unwin, S. C., Cohen, M. H., Pearson, T. J., Seielstad, G. A., Simon, R. S., Linfield, R. P., and Walker, R. C. 1983, *Ap. J.*, **271**, 536.
van der Laan, H. 1966, *Nature*, **211**, 1131.
Wampler, E. J. 1967, *Ap. J.*, **147**, 1.
Wills, B. J., *et al.* 1983, *Ap. J.*, **274**, 62.
Wills, B. J., Netzer, H., and Wills, D. 1985, *Ap. J.*, **288**, 94.

H. D. Aller, M. F. Aller, and P. E. Hodge: Department of Astronomy, University of Michigan, 953 Physics-Astronomy Building, Ann Arbor, MI 48109

T. J. Balonek: Hopkins Observatory, Department of Physics and Astronomy, Williams College, Williamstown, MA 01267

R. E. Barvainis and J. N. Bregman: National Radio Astronomy Observatory, Edgemont Road, Charlottesville, VA 22901

J. D. Bregman, T. P. L. Roellig, and F. C. Witteborn: Space Science Division, NASA/Ames Research Center, Moffett Field, CA 94035

W. A. DENT: Department of Physics and Astronomy, GR Tower B, University of Massachusetts, Amherst, MA 01003

J. ELIAS, C. D. IMPEY, K. MATTHEWS, G. NEUGEBAUER, and B. T. SOIFER: Division of Physics, Mathematics, and Astronomy, Caltech, Pasadena, CA 91125

A. E. GLASSGOLD and P. J. HUGGINS: Physics Department, New York University, 4 Washington Place, New York, NY 10003

J. A. HACKWELL: Department of Physics and Astronomy, University of Wyoming, University Station, Box 3905, Laramie, WY 82071

W. H.-M. KU: Columbia Astrophysics Laboratory, Columbia University, New York, NY 10027

R. J. LEACOCK, A. G. SMITH, and J. WEBB: Department of Astronomy, University of Florida, Gainesville, FL 32611

M. J. LEBOFSKY, G. H. RIEKE, and W. Z. WIŚNIEWSKI: Steward Observatory, University of Arizona, Space Sciences Building, Tucson, AZ 85721

D. F. LESTER, B. J. WILLS, and D. WILLS: Department of Astronomy, University of Texas, RLM 15.308, Austin, TX 78712

A. J. PICA: Department of Physical Science, Salisbury State College, Salisbury, MD 21801

J. T. POLLOCK: Department of Physics and Astronomy, Appalachian State University, Boone, NC 28608